Microwave and Submillimeter-wave Spectra of the Mixed Deuterated-Protonated Water-Dimer Isotopomers

7 AUTHORS, INCLUDING:

G.T. Fraser

National Institute of Standards and Te…

93 PUBLICATIONS **2,376** CITATIONS

SEE PROFILE

Francis J. Lovas

National Institute of Standards and Te…

287 PUBLICATIONS **9,036** CITATIONS

SEE PROFILE

R.D. Suenram

University of Virginia

247 PUBLICATIONS **6,689** CITATIONS

SEE PROFILE

Alex Grushow

Rider University

30 PUBLICATIONS **419** CITATIONS

SEE PROFILE

Microwave and Submillimeter-wave Spectra of the Mixed Deuterated–Protonated Water-Dimer Isotopomers

G. T. Fraser,* F. J. Lovas,* R. D. Suenram,* E. N. Karyakin,† A. Grushow,‡,1
W. A. Burns,‡ and K. R. Leopold‡

*Optical Technology Division, National Institute of Standards and Technology, Gaithersburg, Maryland 20899; †Molecular Spectroscopy Laboratory,
Applied Physics Institute, Nizhnii Novogorod, Russia; and ‡Department of Chemistry, University of Minnesota, Minneapolis, Minnesota 55455

The microwave and submillimeter-wave rotation-tunneling spectra of several mixed deuterated–protonated isotopomers of the water dimer have been measured up to 460 GHz using an electric-resonance optothermal spectrometer, a pulsed-nozzle Fourier-transform microwave spectrometer, and a far-infrared CO_2-laser difference-frequency spectrometer. Spectra were recorded for the *a*-type $K_a = 0–0$ and $1–1$ and *b*- and/or *c*-type $K_a = 1–0$ bands for H_2O—DOD, D_2O—HOH, D_2O—DOH, H_2O—HOD, D_2O—HOD, H_2O—DOH, DHO—HOH, and DHO—DOD, where O—D or O—H denotes the two atoms directly involved in the hydrogen bonding. Spectra of D_2O—HOH, H_2O—HOD, D_2O—HOD, and HDO—HOH, which are higher-energy isomers of H_2O—DOD, H_2O—DOH, D_2O—DOH, and H_2O—DOH, respectively, have not been reported previously. These higher-energy isomers are not significantly populated in Ar molecular beams, such as used in many of the previous microwave studies. Here, we obtain information on two of the three major tunneling processes found in the water dimer, the tunneling interchange of the two protons/deuterons on the proton-acceptor subunit and the tunneling interchange of the two protons/deuterons on the proton-donor subunit. The observed rotation-tunneling selection rules are consistent with previously proposed pathways for these tunneling processes. For H_2O—DOD, D_2O—HOH, and DHO—HOH we find donor interchange tunneling splittings of 24.4(11), 864.14(29), and 1809.39(9) MHz, respectively, averaged over $K_a = 0$ and 1, and for DHO—DOD we find a donor-interchange tunneling splitting of 16.8(1) MHz for $K_a = 0$. For DHO—DOD we also determined the proton/deuteron acceptor interchange tunneling splitting for $K_a = 0$ as 107 723.7(1) MHz, similar to the 117 441.0(2) MHz valued determined previously for DHO—HOD. Because the position of the D/H involved in the hydrogen bonding is nearly coincident with the center of mass of the dimer, isotopomers which only differ by isotopic nuclei at this position have strikingly similar spectra. The present measurements furnish rotational constant and tunneling splitting data to use in the testing and refinement of proposed intermolecular potentials describing water dimer. © 1997 Academic Press

I. INTRODUCTION

An accurate model for the intermolecular potential of H_2O is critical to the theoretical understanding of a number of chemical and physical phenomena in the gas and condensed phases. Molecular spectroscopy offers the opportunity for the precise determination of the H_2O pair potential through the direct least-squares fitting of high-resolution spectroscopic data to a suitable model Hamiltonian. The utility of this approach has been amply tested for the weakly anisotropic intermolecular potentials characteristic of the rare-gas-hydrogen and rare-gas-hydrogen-halide complexes (*1*). Potential modeling of spectroscopic data for more strongly anisotropic systems offers new challenges due to the necessity of using large free-rotor basis sets in the construction of the bending vibrations and due to spectroscopic difficulties arising from the small overlap between the zero-point vibrational wa-

vefunction and the wavefunctions for vibrations localized away from the dimer minimum. To circumvent the latter problem, the regions of the potential not directly explored experimentally can be constrained by results from high-level *ab initio* electronic-structure calculations.

Because of recent advances in computer speed and computational algorithms and due to the increased availability of infrared, far-infrared, and microwave data on a large number of vibration-tunneling states of dimers, efforts have been undertaken to investigate quantitatively the interaction potentials of more anisotropic systems, such as the dimers of hydrogen fluoride (*2, 3*), hydrogen chloride (*4*), ammonia (*5, 6*), and water (*7–9*). Mostly, the potential modeling efforts have not directly least-squares fit the data, but rather tested *ab initio* or model potentials and in some cases made small corrections to these potentials to bring them in better accord with experiment.

In the next few years it is expected that increased computational capabilities will allow the determination of a spectroscopic pair-potential for water. This statement is true provided that sufficient experimental data exists to broadly sam-

A   B
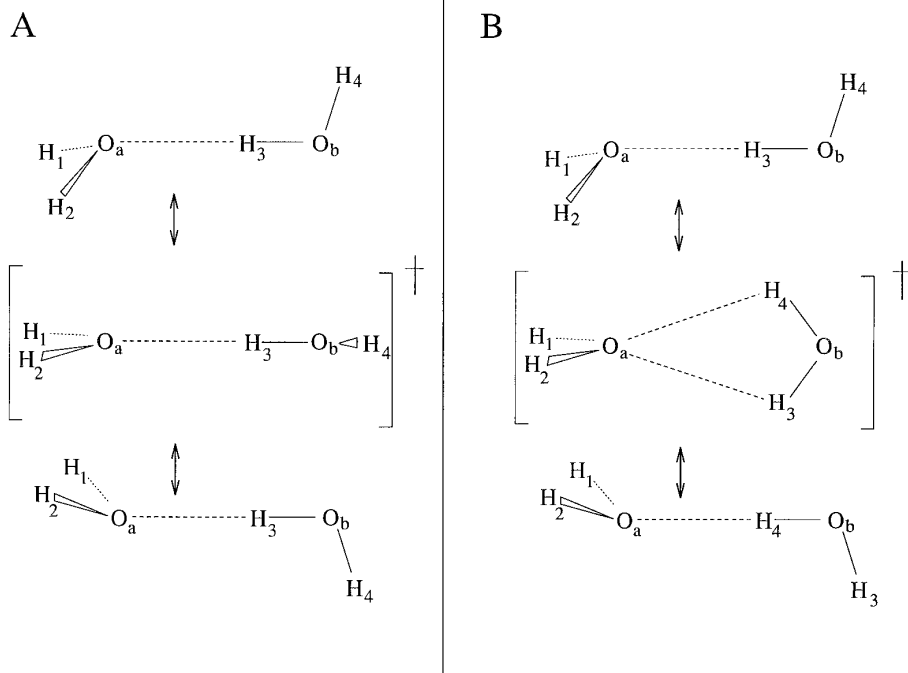
FIG. 1. The two proposed tunneling pathways for the water dimer (*37, 38*) which lead to interchange of the protons on the acceptor (A) or the donor (B).

ple the intermolecular potential. In the present work we significantly increase the spectroscopic data base on the water dimer (*10–31*) by systematically studying the microwave spectra of eight of the twelve possible protonated–deuterated isotopomers. In particular, we provide the first measurements on the higher energy isotopomers, D_2O—HOH, H_2O—HOD, D_2O—HOD, and HDO—HOH, in addition to further measurements on H_2O—DOD, D_2O—DOH, DHO—DOD, and H_2O—DOH. In a previous report (*31*) we discussed similar experiments on the two isomers of $(HOD)_2$.

The water dimer is perhaps the most spectroscopically studied (*32*) hydrogen-bonded complex, with a large experimental (*10–31*) and theoretical (*7–9, 33–38*) effort expended in order to unravel the complex tunneling dynamics present in this system. These tunneling processes allow each of the protons to participate in the hydrogen bonding. The spectroscopic consequence of this tunneling (*33*) is that each rotational-vibrational state of a hypothetical rigid C_s-symmetry dimer is split into six tunneling sublevels. The dominant tunneling process (*13*) resembles the coupled amine-inversion methyl-group internal-rotation motion in methyl amine, and is shown in Fig. 1A.

The methyl-amine-type internal-rotation motion is present in all the isotopomers of water dimer, even those without a plane of symmetry, such as DHO—DOD. Because of the nuclear-spin and electric-dipole selection rules, this tunneling splitting can only be directly measured for the non-

C_s isotopomers, DHO—DOD, DHO—HOH, DHO—HOD, and DHO—DOH. For DHO—HOD and DHO—DOH this splitting is found to be 117 440.97(17) and 214 208.38(23) MHz, respectively, for $K_a = 0$, and approximately a factor of 2 smaller for $K_a = 1$ (*31*).

The second most important tunneling process interchanges the bonding roles of the hydrogen-bond donor and acceptor units and is only present in $(H_2O)_2$, $(D_2O)_2$, and the two isotopomers of $(HOD)_2$, all of which have equivalent donor and acceptor units. The tunneling splittings range from 1172.115(14) (*22*) for $(D_2O)_2$ to 22 554.37(30) MHz (*20*) $(H_2O)_2$. The third most important tunneling process interchanges the positions of the protons or deuterons on the donor unit, as shown schematically in Fig. 1B. This motion, which is also observed in other complexes of H_2O, including OC—HOH (*39*) and H_3N—HOH (*40*), is only allowed in the water dimer complexes in which a H_2O or D_2O unit is the proton donor.

Below, we present our results on the microwave and submillimeter-wave spectra of the protonated/deuterated isotopomers of water dimer. For H_2O—DOD, D_2O—DOH, H_2O—HOD, H_2O—DOH, and DHO—DOD, we completely characterize the $K_a = 0$ and 1 states of the ground vibrational states of the isotopomers. For the other isotopomers, D_2O—HOH, D_2O—HOD, and DHO—HOH, our measurements are less complete, providing only a partial picture of the $K_a = 0$ and 1 energy-level structure. When coupled with the

appropriate dynamical calculations, the present studies offer a valuable test of any theoretical or empirical potential proposed for the water–water interaction.

II. EXPERIMENTAL

Microwave and submillimeter-wave spectra of the various deuterated isotopomers of the water dimer were obtained using a molecular-beam electric-resonance optothermal spectrometer (EROS) (*20, 41*), as described previously in our paper on the $(HOD)_2$ (*31*). The molecular beam is formed by expanding He gas saturated with partially deuterated water vapor through a 40-μm pinhole nozzle at a backing pressure of ~300 kPa. The resulting rotational temperature of the dimers in the molecular beam is estimated from previous studies to be approximately 7 K. The molecular beam is collimated by a 1 mm diameter skimmer and then state-selected by a 56-cm-long electrostatic lens of quadrupolar symmetry. The quadrupole field focusses molecules in ''positive'' Stark states onto a 1.7-K liquid-He-cooled bolometer detector (*42*), while deflecting molecules in ''negative'' Stark states out of the molecular beam. Here, we follow standard convention and use ''positive'' and ''negative'' to refer to the sign of the energy change of a rotational-tunneling state of a molecule when it is placed in an electric field.

Between the nozzle and skimmer, microwave or submillimeterwave radiation is applied to the molecular beam using a section of *K*-band waveguide. A radiofrequency antenna (*43*) is also available for double-resonance studies. The present spectra are dominated by $K_a = 1–0$, $J'–J''$ transitions. To assign *J* and isotopic labels to these transitions, radiofrequency–microwave double resonance is used by monitoring the signal strength of the microwave or submillimeter-wave $K_a = 1–0$ line while searching with the radiofrequency oscillator for the asymmetry doublet transition at $\nu \cong (B - C)J'(J' + 1)/2$. Commercially available microwave synthesizers and frequency doublers supply radiation below 118 GHz, while a phase-locked submillimeter-wave synthesizer based on backward-wave oscillators are used above 150 GHz (*44*). A sample spectrum for DHO—HOH is shown in Fig. 2.

Measurements were also made using a Balle–Flygare pulsed-nozzle Fourier-transform microwave spectrometer (*45*) and a TUFIR far-infrared laser system (*46*), both of which have been described in detail elsewhere. The pulsed-nozzle Fourier transform microwave spectrometer at NIST (*47–49*) operates between 8–26 GHz at a resolution of ~2 kHz at 10 GHz. Both Ar and 10% by volume He in Ne are used as carrier gases. In the case of the Ar gas mixture the rotational temperature is ~1 K, while the He–Ne mixture is significantly warmer, on the order of 3 K. The higher temperature of the He–Ne expansion allows the study of two of the higher energy isotopomers, H_2O—HOD and HDO—HOH, initially only observed in the EROS study.
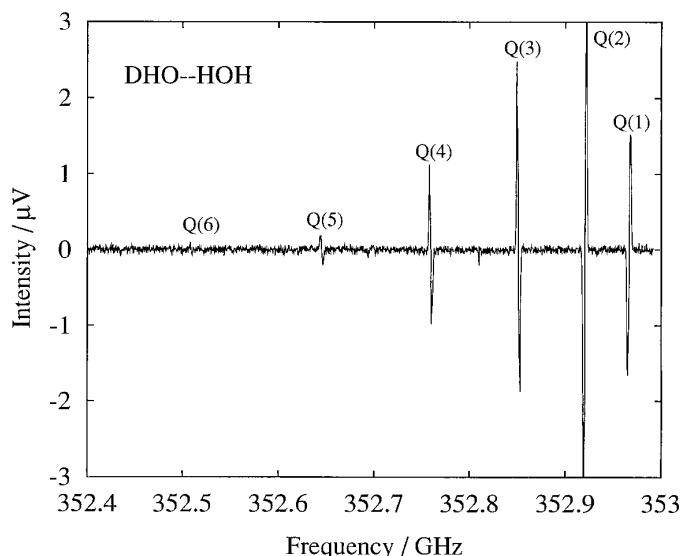

FIG. 2. Spectrum showing a Q branch of one of the $K_a = 1–0$ subbands of DHO—HOH. The spectrum was acquired in less than 6 min. of signal averaging time using a time constant of 125 msec.

The TUFIR spectrometer (*50, 51*) produces submillimeter radiation by mixing the beams from two CO_2 lasers with the output of a microwave oscillator using a tungsten–cobalt point-contact diode. The resulting radiation is directed through the molecular beam produced from a 7.6 cm × 0.05 mm slit nozzle and then detected by a liquid-He-cooled bolometer detector. In the present study, the TUFIR spectrometer was used to record most of the spectrum of the 400-GHz band of H_2O—DOH, which is out of range of the backward-wave oscillators available in the EROS study.

III. RESULTS

A. H_2O—DOD

The observed transitions for H_2O—DOD are listed in Table 1. An energy-level diagram showing the rotation-tunneling levels studied for $J = 0$, $K_a = 0$ and $J = 1$, $K_a = 1$ is presented in Fig. 3. The rotation-tunneling symmetries and statistical weights are also given in the figure. The molecular symmetry group for H_2O—DOD is G_8, and has been discussed previously by Coudert and Hougen (*36*). Unlike the G_{16} group of $(H_2O)_2$, the G_8 group has no E symmetry species. The selection rules are $A_2^+ \leftrightarrow A_2^-$, $A_1^+ \leftrightarrow A_1^-$, $B_2^+ \leftrightarrow B_2^-$, and $B_1^+ \leftrightarrow B_1^-$. For convenience, we label the four $K_a = 0$ tunneling states 0 through 3 and the four $K_a = 1$ tunneling states 4 through 7. The methyl-amine-like tunneling motion splits states 0 and 1 from 2 and 3 and states 4 and 5 from 6 and 7. The proton-donor interchange tunneling motion splits states 0 from 1, 2 from 3, 4 from 5, and 6 from

TABLE 1
Measured Transition Frequencies for H_2O—DOD[a]

n[b]	$J_{K_aK_c}$	s	n	$J_{K_aK_c}$	s	ν (MHz)	n	$J_{K_aK_c}$	s	n	$J_{K_aK_c}$	s	ν (MHz)
5	5_{14}	B_2^+	5	5_{15}	B_2^-	85.11	5	2_{11}	B_2^-	2	3_{03}	B_2^+	64084.37
4	5_{14}	A_2^+	4	5_{15}	A_2^-	86.04	4	5_{15}	A_2^-	3	5_{05}	A_2^+	99350.80
4	6_{15}	A_2^-	4	6_{16}	A_2^+	120.10	4	4_{14}	A_2^+	3	4_{04}	A_2^-	99358.15
6	2_{11}	B_1^-	6	2_{12}	B_1^+	151.30	4	3_{13}	A_2^-	3	3_{03}	A_2^+	99363.80
7	2_{11}	A_1^-	7	2_{12}	A_1^+	151.58	4	2_{12}	A_2^+	3	2_{02}	A_2^-	99368.00
7	3_{12}	A_1^+	7	3_{13}	A_1^-	303.30	4	1_{11}	A_2^-	3	1_{01}	A_2^+	99371.05
7	4_{13}	A_1^-	7	4_{14}	A_1^+	505.18	5	5_{15}	B_2^-	2	5_{05}	B_2^+	99400.70
7	5_{14}	A_1^+	7	5_{15}	A_1^-	757.85	5	4_{14}	B_2^+	2	4_{04}	B_2^-	99408.60
2	1_{01}	B_2^+	2	0_{00}	B_2^-	11785.31	5	3_{13}	B_2^-	2	3_{03}	B_2^+	99414.70
3	1_{01}	A_2^+	3	0_{00}	A_2^-	11785.31	5	2_{12}	B_2^+	2	2_{02}	B_2^-	99419.05
0	1_{01}	A_1^-	0	0_{00}	A_1^+	11789.49	4	1_{10}	A_2^+	3	0_{00}	A_2^-	111161.93
1	1_{01}	B_1^-	1	0_{00}	B_1^+	11789.49	4	5_{14}	A_2^+	3	4_{04}	A_2^-	158344.21
3	2_{02}	A_2^-	3	1_{01}	A_2^+	23569.655	5	5_{14}	B_2^+	2	4_{04}	B_2^-	158393.41
2	2_{02}	B_2^-	2	1_{01}	B_2^+	23569.782	4	6_{15}	A_2^-	3	5_{05}	A_2^+	170139.74
1	2_{02}	B_1^+	1	1_{01}	B_1^-	23577.787	5	6_{15}	B_2^-	2	5_{05}	B_2^+	170188.31
0	2_{02}	A_1^+	0	1_{01}	A_1^-	23577.985	4	7_{16}	A_2^+	3	6_{06}	A_2^-	181933.92
4	5_{14}	A_2^+	3	6_{06}	A_2^-	28758.59	5	7_{16}	B_2^+	2	6_{06}	B_2^-	181981.20
5	5_{14}	B_2^+	2	6_{06}	B_2^-	28807.27	7	3_{13}	A_1^-	0	4_{04}	A_1^+	203988.99
5	3_{13}	B_2^-	5	2_{12}	B_2^+	35347.60	6	2_{12}	B_1^+	1	3_{03}	B_1^-	215798.50
4	3_{13}	A_2^-	4	2_{12}	A_2^+	35347.80	7	2_{12}	A_1^+	0	3_{03}	A_1^-	215846.10
3	3_{03}	A_2^+	3	2_{02}	A_2^-	35352.22	7	1_{11}	A_1^-	0	2_{02}	A_1^+	227681.36
2	3_{03}	B_2^+	2	2_{02}	B_2^-	35352.22	6	2_{11}	B_1^-	1	2_{02}	B_1^+	251313.51
5	3_{12}	B_2^+	5	2_{11}	B_2^-	35364.60	7	2_{11}	A_1^-	0	2_{02}	A_1^+	251362.18
4	3_{12}	A_2^+	4	2_{11}	A_2^-	35364.60	7	3_{12}	A_1^+	0	3_{03}	A_1^-	251439.87
4	4_{13}	A_2^-	3	5_{05}	A_2^+	40508.20	6	4_{13}	B_1^-	1	4_{04}	B_1^+	251496.48
5	4_{13}	B_2^-	2	5_{05}	B_2^+	40557.75	7	4_{13}	A_1^-	0	4_{04}	A_1^+	251544.08
2	5_{05}	B_2^+	2	4_{04}	B_2^-	58907.60	6	5_{14}	B_1^+	1	5_{05}	B_1^-	251627.38
3	5_{05}	A_2^+	3	4_{04}	A_2^-	58907.60	7	5_{14}	A_1^+	0	5_{05}	A_1^-	251674.30
4	5_{14}	A_2^+	4	4_{13}	A_2^-	58927.73	7	6_{15}	A_1^-	0	6_{06}	A_1^+	251830.05
0	5_{05}	A_1^-	0	4_{04}	A_1^+	58927.73	7	7_{16}	A_1^+	0	7_{07}	A_1^-	252012.02
5	5_{14}	B_2^+	5	4_{13}	B_2^-	58927.73	7	4_{14}	A_1^+	0	3_{03}	A_1^-	298186.83
1	5_{05}	B_1^-	1	4_{04}	B_1^+	58927.73	6	5_{15}	B_1^-	1	4_{04}	B_1^+	309798.40
4	2_{11}	A_2^-	3	3_{03}	A_2^+	64033.19	7	5_{15}	A_1^-	0	4_{04}	A_1^+	309843.83

[a] Uncertainties are 0.25 MHz. For transitions given with three digits to the right of the decimal point the uncertainties are 0.01 MHz.
[b] Refer to Figure 3 for definition of n.

7. The remaining splitting in the figure for $K_a = 1$ is due to asymmetry doubling.

As seen in the table and figure, four $K_a = 1$–0 bands are observed for H_2O—DOD. These observations allow complete characterization of the $K_a = 0$ and 1 rotation-tunneling states for the ground vibrational state of the isotopomer. Two of the bands have b-type electric-dipole selection rules while the other two bands have c-type selection rules. The change in selection rules for the two sets of bands is a consequence of the large amplitude motions which cause a dynamic reversal of the b and c inertial axes for the different tunneling states. The two b-type bands and the two c-type bands each have 2:1 relative intensities, consistent with the 6:3 or 18:9 nuclear-spin statistical weight ratios shown in the figure. The observed transition selection rules are symmetric–antisymmetric in both of the tunneling states, the methyl-amine-like tunneling which interchanges the two

equivalent protons, and the donor-proton tunneling which interchanges the two deuterons. For both motions, the tunneling pathways in Fig. 1 have the electric dipole moment operator as an antisymmetric function of each tunneling coordinate. The experimental tunneling-state selection rules are thus consistent with the pathways shown in Fig. 1.

The observed transitions in Table 1 were least-squares fit to the frequencies calculated from the energy-level expression,

$$E(J, K, n) = E_n + \bar{B}_n[J(J + 1) - K_a^2]$$
$$- D_n[J(J + 1) - K_a^2]^2 - \delta_{1,K_a} (-1)^{K_a+K_c} \quad [1]$$
$$\times \left[\frac{(B - C)_n}{4} - d_n J(J + 1) \right] J(J + 1),$$

where E_n is the hypothetical $J = 0$ energy origin for the nth K_a-tunneling state, $\bar{B}_n = (B + C)_n/2$ and $(B - C)_n$ are rota-
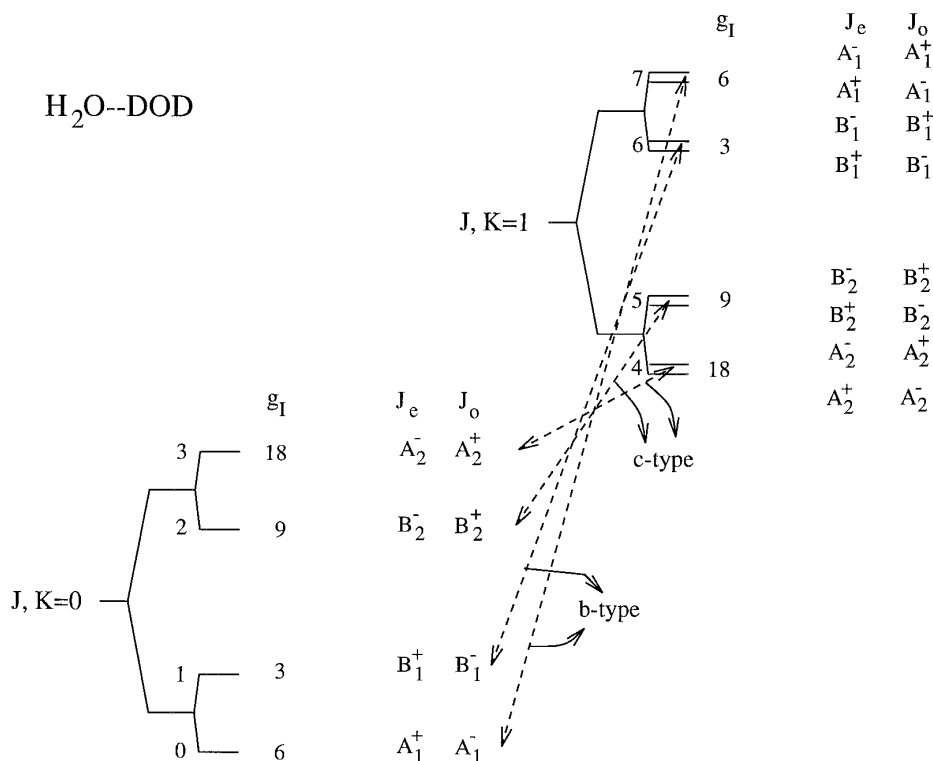
FIG. 3. Energy-level diagram for the $J = 0$, $K_a = 0$ and $J = 1$, $K_a = 1$ rotational states of the ground vibrational state of H_2O—DOD showing the splitting of each rotational states into four tunneling components. The largest tunneling splittings results from a tunneling motion which interchanges the two protons on the donor unit through a pathway as shown in Fig. 1A. The other tunneling splitting originates from the interchange of the deuterons on the donor unit via the pathway pictured in Fig. 1B. The remaining splitting for $K_a = 1$ is due to asymmetry doubling. The symmetries of the rovibronic species are shown for even and odd J and the nuclear spin statistical weights, g_I, are also listed. The observed $K_a = 1-0$ bands and types are shown by dotted lines.

tional constants, and D_n and d_n are centrifugal distortion constants on $\bar{B}_n$ and $(B - C)_n$, respectively. The spectroscopic constants determined from the fit are given in Table 2. The standard deviation of the fit of 0.21 MHz is within our typical measurement precision of 0.25 MHz. The presence of four different nuclear-spin modifications for the dimer results from the four combinations of the two nuclear-spin modifications of H_2O with the two nuclear-spin modifications of D_2O. The relative energy differences between these modifications cannot be determined in the present experiments. We thus arbitrarily constrain the E_n for states 0 through 3 at zero. The nuclear-spin/symmetry constraints on the selection rules further allows only the relative energies of 7 with respect to 0, 6 with respect to 1, 5 with respect to 2, and 4 with respect to 3 to be determined.

The energy origins in Table 2 can be used to estimate the magnitude of the tunneling splitting associated with the proton-donor deuteron interchange motion. This splitting is just the separation of the $n = 1$ and 0, $n = 3$ and 2, $n = 5$ and 4, and $n = 7$ and 6 states in the energy-level diagram of Fig. 3. Because of the observed selection rules, the estimated values

for the tunneling splitting are averaged over the $K_a = 0$ and 1 states, and are obtained from $[E_1 - E_0 + E_7 - E_6]/2$ and $[E_3 - E_2 + E_5 - E_4]/2$, using the values for the E_i given in the table. For H_2O—DOD we obtain a tunneling splitting of 24.4(11) MHz from the two higher frequency bands and a splitting of 25.7(9) MHz from the two lower frequency bands. For $(D_2O)_2$ these tunneling splittings have been estimated as 14.0 and 13.4 MHz for the higher and lower frequency bands, respectively. The near factor of two difference in tunneling splitting between $(D_2O)_2$ and H_2O—DOD is indicative of the role played by the protons/deuterons of the proton-acceptor subunit in the tunneling motion, as anticipated from the tunneling pathway presented in Fig. 1.

A similar analysis cannot be used to estimate the tunneling splitting associated with the methyl-amine-like motion, since this splitting is known to have a large K_a dependence, as inferred from studies of HDO—DOD (30) and (HDO)$_2$ (31). Moreover a direct measure of this tunneling splitting via $\Delta K_a = 0$ transitions is not possible due to the selection rules. The equilibrium configurations of HDO—DOD and (HDO)$_2$ do not have a plane of symmetry and thus additional $K_a = 1-0$

TABLE 2
Spectroscopic Constants in MHz for Isotopomers of Water Dimer[a,b,c]

n[d]	E_n	$\overline{B}_n$	D_n	$(B-C)_n$
H_2O–DOD $\sigma = 0.21$				
0	0.0	5894.8227(33)	0.04087(29)	0.0
1	0.0 [e]	5894.7739(32)	0.04087(29)	0.0
2	0.0 [e]	5892.7674(24)	0.04027(13)	0.0
3	0.0 [e]	5892.7358(24)	0.04027(13)	0.0
4	105265.78(11)	5893.3973(92)	0.04135(16)	5.7257(68)
5	105317.27(15)	5893.360(10)	0.04135(16)	5.6742(96)
6	257130.50(18)	5895.157(14)	0.04094(41)	50.409(19)
7	257179.20(14)	5895.112(14)	0.04094(41)	50.5285(88)
D_2O–HOH $\sigma = 0.39$				
0	0.0	5681.575(61)	0.0456(13)	0.0
1	0.0 [e]	5681.502(53)	0.0456(13)	0.0
6	256293.41(23)	5688.162(53)	0.0456(13)	77.409(24)
7	258017.68(54)	5687.937(78)	0.0456(13)	76.850(39)
D_2O–DOH $\sigma = 0.19$				
0	0.0	5674.9603(41)	0.04321(54)	0.0
1	0.0 [e]	5672.6942(50)	0.03455(70)	0.0
2	45173.88(12)	5676.3531(31)	0.04764(45)	132.0718(52)
3	247077.16(11)	5681.586(18)	0.04068(72)	77.704(29)
H_2O–HOD $\sigma = 0.20$				
0	0.0	5894.785(21)	0.04195(45)	0.0
1	0.0 [e]	5886.8077(41)	0.03212(30)	0.0
2	102404.74(11)	5892.1724(83)	0.04204(22)	12.050(16)
3	261898.49(11)	5894.546(22)	0.04144(40)	52.905(11)
D_2O–HOD $\sigma = 0.12$				
0	0.0	5435.047(12)	0.03653(28)	0.0
3	165661.971(62)	5435.272(14)	0.03653(28)	32.0154(87)
H_2O–DOH $\sigma = 0.44$				
0	0.0	6156.3537(59)	0.04710(56)	0.0
1	0.0 [e]	6164.3301(70)	0.04118(77)	0.0
2	28407.38(35)	6150.015(40)	0.05081(96)	53.862(20)
3	425103.43(22)	6161.186(27)	0.04660(74)	3.387(39)
DHO–HOH $\sigma = 0.27$				
0	0.0	5905.2459(39)	0.04869(19)	0.0
1	0.0 [e]	5905.2459(39)	0.04869(19)	0.0
6	358895.11(11)	5905.9024(68)	0.04869(19)	48.832(12)
7	362513.88(13)	5905.625(10)	0.04869(19)	47.676(22)
DHO–DOD $\sigma = 0.25$				
0	0.0	5648.2598(32)	0.03861(30)	0.0
1	0.0 [e]	5648.2622(33)	0.03903(30)	0.0
2	107706.92(15)	5645.213(20)	0.03758(51)	0.0
3	107740.556(98)	5645.1761(50)	0.03772(24)	0.0
4	182425.32(11)	5650.089(10)	0.04013(35)	61.208(15)
5	182413.54(13)	5650.125(13)	0.04062(42)	61.169(16)
6	225401.28(11)	5644.616(15)	0.03895(36)	17.789(12)
7	225425.74(11)	5644.560(10)	0.03818(23)	17.711(12)

[a] Uncertainties are one standard deviation from the least squares fit.
[b] Constants without uncertainties are constrained in the fit.
[c] The following constraints were used in the fits: for H_2O–DOD, $D_0 = D_1$, $D_2 = D_3$, $D_4 = D_5$, and $D_6 = D_7$; for D_2O–HOH, $D_0 = D_1 = D_6 = D_7$; for D_2O–HOD, $D_0 = D_3$; and for DHO–HOH $D_0 = D_1 = D_6 = D_7$.
[d] The state label n is defined in Figures 3 - 10.
[e] The energy of this state with respect to $n = 0$ is not determined.

bands and Coriolis driven $K_a = 1-1$ and $0-0$ bands are allowed across the tunneling gap, giving a direct measure of the methylamine tunneling splitting for $K_a = 0$ and 1. In the case of HDO—HOD, for example, the methyl-amine tunneling splitting changes from 117 to 46 GHz from $K_a = 0$ to $K_a = 1$.

B. D_2O—HOH

The analysis on D_2O—HOH parallels that of H_2O—DOD. The energy-level diagram and observed $K_a = 1-0$ bands for D_2O—HOH are shown in Fig. 4. The D_2O—HOH isotopomer is higher in energy than the H_2O—DOD form, as verified by our inability to observe the higher energy species with the Fourier-transform microwave spectrometer at the $T_{rot} = 1$ K beam temperature of an Ar expansion. The energy difference between the two forms is presumably dominated by the differences in the zeropoint frequencies of the O—HO and O—DO bending vibrations. The molecular-symmetry groups for both molecules are G_8, leading to energy-level diagrams which are qualitatively similar, as seen by comparison of Figs. 3 and 4.

For D_2O—HOH, only two of the four $K_a = 1-0$ bands predicted for this molecule are assigned, with the observed transition frequencies listed in Table 3. The two bands expected from the $n = 2$ and 3 states could not be identified in our spectrum, despite the fact that the $n = 2$ and 3 states should be populated since the collisional relaxation of these two states to the $n = 0$ and 1 states is nuclear-spin and symmetry forbidden. The two observed bands are both c-type, in contrast to the b-type selection rules seen for D_2O—HOH. This change in selection rules between the two isotopomers is not surprising since a rigid-molecule structural model predicts that the c-inertial axis will be normal to the symmetry plane for D_2O—HOH and the b-inertial axis will be normal to this plane for H_2O—DOD. The relative intensities for the two bands are consistent with the expected 6:3 statistical weight ratio.

The spectroscopic constants resulting from a least-squares fit of the data in Table 2 to the energy-level expression of Equation 1 are listed in Table 2. Because of the nuclear-spin statistics, the precise energy difference between states 0 and 1 could not be determined. The energies of these two states were thus constrained to zero in the fit. A rough value for the energy separation of the two states can be obtained from the frequency difference of the two observed bands. We must first assume that the K_a dependence of the proton-donor proton-interchange tunneling splitting is small. We find a tunneling splitting of 862.14(29) MHz averaged over $K_a = 0$ and 1, suggesting that the separation of the $n = 1$ and 0 states is on the order of 850 MHz. For $(H_2O)_2$ previous measurements determine the proton-donor interchange tunneling splitting to be 1395.2(3) MHz with a K_a dependence of 60.6(4) × K_a^2 MHz.

C. D_2O—DOH

The energy-level diagram for D_2O—DOH is simplified from that of H_2O—DOD and D_2O—HOH since the tunneling associated with the interchange of the two donor protons or deuterons is no longer present. The molecular symmetry
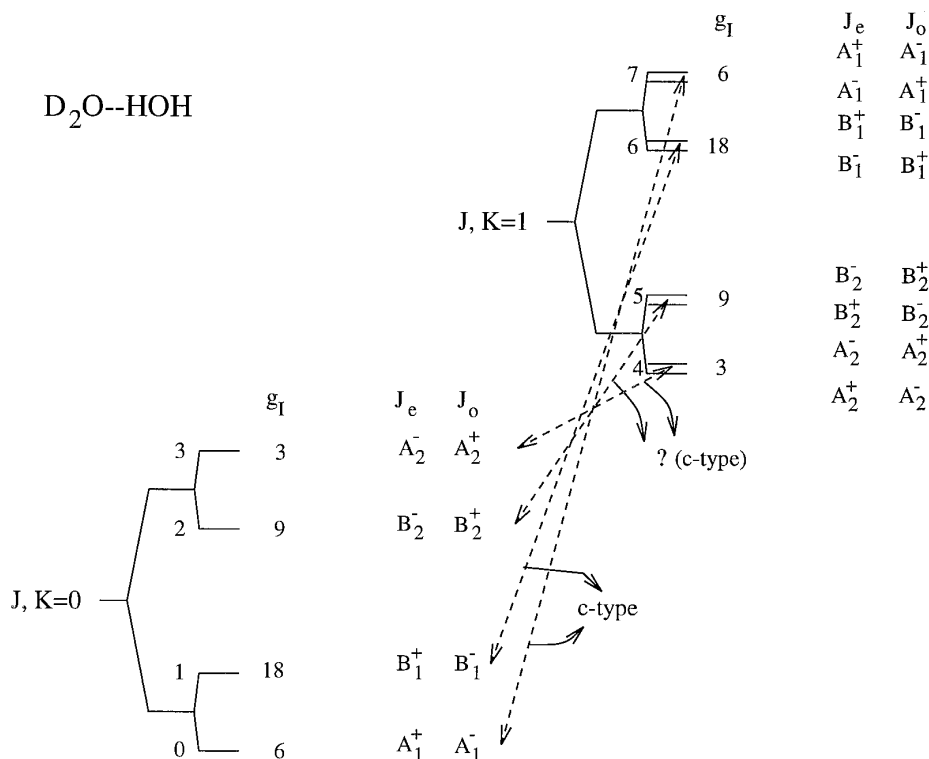
FIG. 4. Energy-level diagram for D_2O—HOH. Note the similarities with the energy level diagram for H_2O—DOD given in Fig. 2. The two c-type bands denoted with a question mark were not directly observed in the present study. The unobserved bands are assumed to be c-type from comparison with D_2O—DOH.

group for D_2O—DOH is G_4 and the energy-level diagram for the dimer is shown in Fig. 5. The statistical weights, g_I, in Figs. 5 through 10 do not include contributions from the nuclear spins of the DOH subunit. To include this contributions all the g_I's in these figures need to be multiplied by a factor of 6.

Four ($n = 0$–3) instead of eight states are possible for D_2O—DOH since the only tunneling motion present is that which interchanges the two deuterons on the acceptor unit, presumably via a pathway similar to that postulated for H_2O—DOD and D_2O—HOH. The selection rules on the rotational-tunneling species are $A_1^+ \leftrightarrow A_1^-$ and $A_2^+ \leftrightarrow A_2^-$. The rotational constants and methyl-amine type tunneling splitting are expected to be similar to those of D_2O—HOH since

TABLE 3
Measured Transition Frequencies for D_2O—HOH^a

n^b	$J_{K_aK_c}$	s	n	$J_{K_aK_c}$	s	ν (MHz)	n	$J_{K_aK_c}$	s	n	$J_{K_aK_c}$	s	ν (MHz)
6	2_{11}	B_1^+	6	2_{12}	B_1^-	232.18	6	3_{13}	B_1^+	1	3_{03}	B_1^-	250453.50
7	3_{12}	A_1^-	7	3_{13}	A_1^+	460.40	6	2_{12}	B_1^-	1	2_{02}	B_1^+	250529.68
6	3_{12}	B_1^-	6	3_{13}	B_1^+	464.29	6	1_{11}	B_1^+	1	1_{01}	B_1^-	250580.38
6	4_{13}	B_1^+	6	4_{14}	B_1^-	773.89	7	4_{14}	A_1^-	0	4_{04}	A_1^+	252074.10
0	5_{05}	A_1^-	0	4_{04}	A_1^+	56792.40	6	2_{11}	B_1^+	1	1_{01}	B_1^-	273486.12
1	5_{05}	B_1^-	1	4_{04}	B_1^+	56792.40	7	2_{11}	A_1^+	0	1_{01}	A_1^-	275208.55
6	4_{13}	B_1^+	1	5_{05}	B_1^-	194335.18	6	3_{12}	B_1^-	1	2_{02}	B_1^+	285002.34
7	4_{13}	A_1^+	0	5_{05}	A_1^-	196049.95	7	3_{12}	A_1^-	0	2_{02}	A_1^+	286722.20
6	3_{12}	B_1^-	1	4_{04}	B_1^+	205478.06	6	4_{13}	B_1^+	1	3_{03}	B_1^-	296567.76
6	2_{11}	B_1^+	1	3_{03}	B_1^-	216677.87	7	4_{13}	A_1^+	0	3_{03}	A_1^-	298284.50
6	4_{14}	B_1^-	1	4_{04}	B_1^+	250353.08	6	5_{14}	B_1^-	1	4_{04}	B_1^+	308180.63

^{a} Uncertainties are 0.25 MHz. For transitions given with three digits to the right of the decimal point the uncertainties are 0.01 MHz.
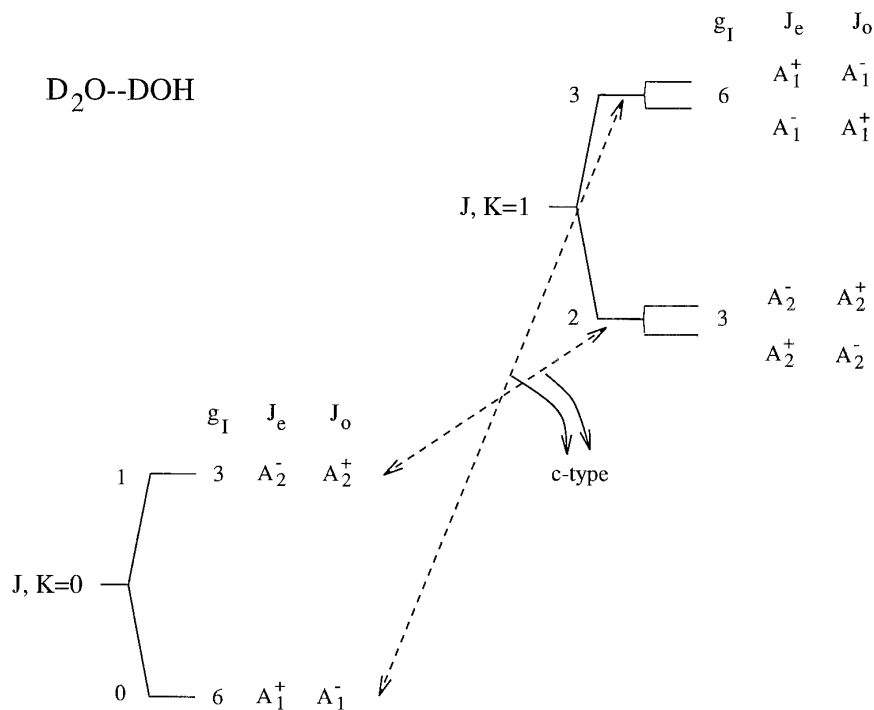^{b} Refer to Figure 4 for definition of n.

FIG. 5. Energy-level diagram for D_2O—DOH. Note the absence of the tunneling splitting associated with the interchange of the two protons/deuterons on the donor unit.

the proton/deuteron which is involved in the hydrogen bond is located close to the center of mass of the complex. Indeed, the spectral assignments for isotopomers which differ only by H or D in the hydrogen bond are greatly facilitated by the similarities in their rotational constants and methyl-amine tunneling splittings.

Both of the expected $K_a = 1-0$ bands are observed for D_2O—DOH, with each having c-type selection rules. The measured transitions are given in Table 4. The experimental selection rules for D_2O—DOH suggest that the two unobserved $K_a = 1-0$ bands for D_2O—HOH should also be c-type. The analysis for D_2O—DOH precedes as before, with the spectroscopic constants summarized in Table 2. As expected, the $\bar{B}$, $B-C$, and E_4 values are similar to those found for D_2O—HOH. As with all the isotopomers, the relative energies of the different nuclear-spin modifications of the dimers are not directly measured. We thus arbitrary fix the lowest energy state of each spin-modification at 0.

D. H_2O—HOD

The analysis of H_2O—HOD is analogous to that of D_2O—HOD. The molecular symmetry group for both molecules is G_4, and the only tunneling process present is the methyl-amine motions which interchanges the two structurally equivalent deuterons on the proton acceptor unit. An energy-level diagram showing the observed transitions is given in

Fig. 6. The observed b/c selection rules for the $K_a = 1-0$ bands are similar to those observed for H_2O—DOD. The $K_a = 0$ and 1 states are completely characterized for the complex. The measured transition frequencies are listed in Table 5 and the spectroscopic constants resulting from the fit of the transitions are listed in Table 2.

E. D_2O—HOD

The energy-level diagram for D_2O—HOD is presented in Fig. 7. Again, the analysis is similar to the of D_2O—DOH, which has the same symmetry and statistical weights. Only the c-type $K_a = 1-0$, $n = 3-0$ band has been observed for D_2O—DOH. The c-type $K_a = 1-0$, $n = 2-1$ band expected near $E_2-E_1 = \sim89$ GHz, from analogy with $(D_2O)_2$, could not be identified. The spectroscopic constants for the $n = 0$ and 3 states and the experimental selection rules are similar to those for $(D_2O)_2$. The spectroscopic constants resulting from the fit of the transitions of Table 6 to the energy level expression of equation 1 are presented in Table 2. For comparison, we have previously measured the $\bar{B}$, $B - C$, and the equivalent to the E_3-E_0 gap for $(D_2O)_2$ to be ~5433 MHz, ~33 MHz, and ~161 GHz, with the precise values dependent on the particular donor-acceptor interchange tunneling state considered.

F. H_2O—DOH

The energy-level diagram for H_2O—DOH is given in Fig. 8 and the measured transitions are listed in Table 7. The energy

TABLE 4
Measured Transition Frequencies for H_2O—DOH^a

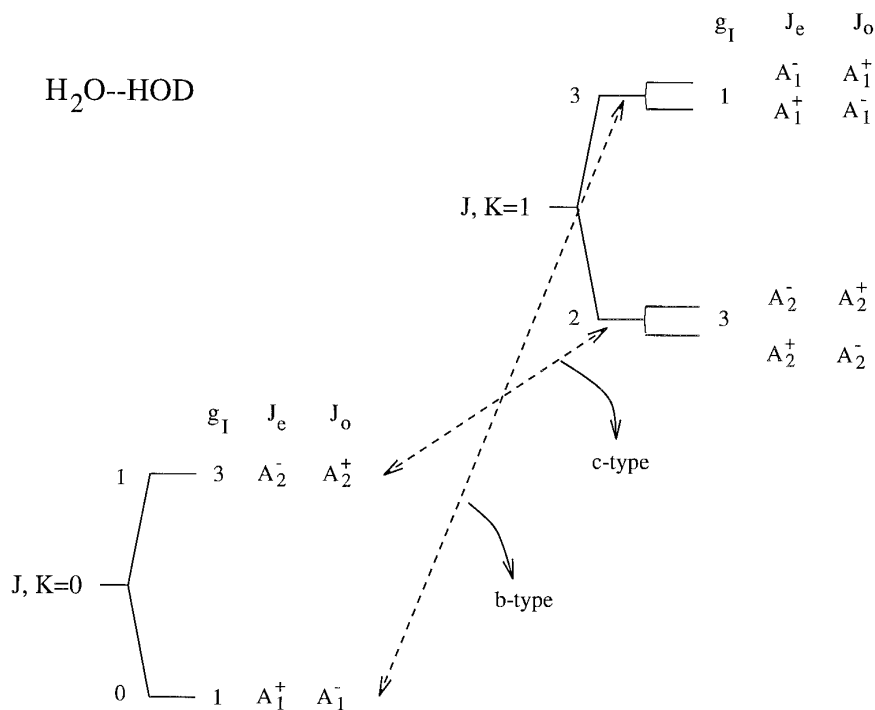| n^b	$J_{K_aK_c}$	s	n	$J_{K_aK_c}$	s	ν (MHz)	n	$J_{K_aK_c}$	s	n	$J_{K_aK_c}$	s	ν (MHz)
3	1_{10}	A_1^-	3	1_{11}	A_1^+	77.76	2	1_{11}	A_2^-	1	1_{01}	A_2^+	39438.89
2	1_{10}	A_2^+	2	1_{11}	A_2^-	132.38	2	4_{13}	A_2^-	1	3_{03}	A_2^+	85600.45
3	2_{11}	A_1^+	3	2_{12}	A_1^-	233.20	2	5_{14}	A_2^+	1	4_{04}	A_2^-	97298.47
2	2_{11}	A_2^-	2	2_{12}	A_2^+	396.26	3	5_{14}	A_1^-	0	6_{06}	A_1^+	174119.58
2	3_{12}	A_2^+	2	3_{13}	A_2^-	792.13	3	4_{13}	A_1^+	0	5_{05}	A_1^-	185191.27
1	1_{01}	A_2^+	1	0_{00}	A_2^-	11345.252	3	3_{12}	A_1^-	0	4_{04}	A_1^+	196320.86
0	1_{01}	A_1^-	0	0_{00}	A_1^+	11349.749	3	2_{11}	A_1^+	0	3_{03}	A_1^-	207507.10
2	2_{12}	A_2^+	2	1_{11}	A_2^-	22572.195	3	1_{10}	A_1^-	0	2_{02}	A_1^+	218749.18
1	2_{02}	A_2^-	1	1_{01}	A_2^+	22689.670	3	6_{16}	A_1^-	0	6_{06}	A_1^+	240865.81
0	2_{02}	A_1^+	0	1_{01}	A_1^-	22698.457	3	5_{15}	A_1^+	0	5_{05}	A_1^-	241016.19
2	2_{11}	A_2^-	2	1_{10}	A_2^+	22836.342	3	3_{13}	A_1^+	0	3_{03}	A_1^-	241243.31
2	3_{13}	A_2^-	2	2_{12}	A_2^+	33855.87	3	1_{11}	A_1^+	0	1_{01}	A_1^-	241370.38
0	3_{03}	A_1^-	0	2_{02}	A_1^+	34045.05	3	1_{10}	A_1^-	0	0_{00}	A_1^+	252797.48
2	3_{12}	A_2^+	2	2_{11}	A_2^-	34251.75	3	2_{11}	A_1^+	0	1_{01}	A_1^-	264251.04
2	2_{12}	A_2^+	1	2_{02}	A_2^-	39321.46							.

^{a} Uncertainties are 0.25 MHz. For transitions given with three digits to the right of the decimal point the uncertainties are 0.01 MHz.
^{b} Refer to Figure 5 for definition of n.

level diagram, statistical weights, and state symmetries are analogous to those of H_2O—HOD. Both of the two expected K_a = 1–0 bands were observed for the complex, with the combination of b- and c-type selection rules and frequency origins agreeing with previous observations on H_2O—HOH. The analysis proceeds as before except that we also include a b-type Coriolis interaction between the nearly degenerate A_2 symmetry $K_a = 0$, $n = 1$ and $K_a = 1$, $n = 2$ states. An analogous Coriolis coupling is present in the other isotopomers but the states involved are nonresonant making the data insensitive to the presence of the interaction. We follow our analysis on H_2O—HOH and use a matrix element of the form

$$\alpha_{1,2}[J(J + 1)]^{1/2}, \qquad [2]$$

FIG. 6. Energy-level diagram for H_2O—HOD.

TABLE 5
Measured Transition Frequencies for H_2O—HOD^a

n^b	$J_{K_aK_c}$	s	n	$J_{K_aK_c}$	s	ν (MHz)	n	$J_{K_aK_c}$	s	n	$J_{K_aK_c}$	s	ν (MHz)
2	1_{10}	A_2^+	2	1_{11}	A_2^-	12.02	2	5_{14}	A_2^+	1	4_{04}	A_2^-	155608.44
2	2_{11}	A_2^-	2	2_{12}	A_2^+	35.90	2	6_{15}	A_2^-	1	5_{05}	A_2^+	167463.35
3	1_{10}	A_1^+	3	1_{11}	A_1^-	52.93	2	7_{16}	A_2^+	1	6_{06}	A_2^-	179324.50
2	3_{12}	A_2^+	2	3_{13}	A_2^-	71.90	2	8_{17}	A_2^-	1	7_{07}	A_2^+	191190.32
2	4_{13}	A_2^-	2	4_{14}	A_2^+	120.65	3	4_{14}	A_1^+	0	5_{05}	A_1^-	196809.70
3	2_{11}	A_1^-	3	2_{12}	A_1^+	158.68	2	9_{18}	A_2^+	1	8_{08}	A_2^-	203057.53
2	5_{14}	A_2^+	2	5_{15}	A_2^-	179.59	3	3_{13}	A_1^-	0	4_{04}	A_1^+	208695.88
2	6_{15}	A_2^-	2	6_{16}	A_2^+	250.93	3	2_{12}	A_1^+	0	3_{03}	A_1^-	220559.20
3	3_{12}	A_1^+	3	3_{13}	A_1^-	317.50	3	1_{10}	A_1^+	0	1_{01}	A_1^-	256030.31
2	7_{16}	A_2^+	2	7_{17}	A_2^-	333.50	3	2_{11}	A_1^-	0	2_{02}	A_1^+	256082.28
1	1_{01}	A_2^+	1	0_{00}	A_2^-	11773.488	3	3_{12}	A_1^+	0	3_{03}	A_1^-	256160.87
1	3_{03}	A_2^+	1	2_{02}	A_2^-	35317.40	3	4_{13}	A_1^-	0	4_{04}	A_1^+	256265.43
1	5_{05}	A_2^+	1	4_{04}	A_2^-	58852.21	3	5_{14}	A_1^+	0	5_{05}	A_1^-	256396.51
2	5_{15}	A_2^-	2	4_{14}	A_2^+	58871.81	3	6_{15}	A_1^-	0	6_{06}	A_1^+	256553.92
2	2_{11}	A_2^-	1	3_{03}	A_2^+	61245.63	3	7_{16}	A_1^+	0	7_{07}	A_1^-	256737.35
2	1_{11}	A_2^-	1	1_{01}	A_2^+	96517.29	3	1_{11}	A_1^-	0	0_{00}	A_1^+	267766.56
2	2_{12}	A_2^+	1	2_{02}	A_2^-	96526.88	3	2_{12}	A_1^+	0	1_{01}	A_1^-	279501.44
2	3_{13}	A_2^-	1	3_{03}	A_2^+	96540.59	3	3_{13}	A_1^-	0	2_{02}	A_1^+	291207.46
2	4_{14}	A_2^+	1	4_{04}	A_2^-	96557.68	3	5_{15}	A_1^-	0	4_{04}	A_1^+	314529.75
2	5_{15}	A_2^-	1	5_{05}	A_2^+	96577.34	3	7_{17}	A_1^-	0	6_{06}	A_1^+	337725.60
2	1_{10}	A_2^+	1	0_{00}	A_2^-	108302.75							

^{a} Uncertainties are 0.25 MHz. For transitions given with three digits to the right of the decimal point the uncertainties are 0.01 MHz.
^{b} Refer to Figure 6 for definition of n.

where $\alpha_{1,2}$ is an effective coupling constant between states with $n = 1$ and 2. To treat the Coriolis interaction, a series of 2×2 matrices are diagonalized for each J, where the diagonal elements are the $E(J, K_a, n)$ of equation 1, with $n = 1$ and 2 and the off-diagonal element is given by Eq. [2] above. The present data set was only weakly sensitive to the magnitude of the Coriolis interaction so in the fits we have constrained $\alpha_{1,2}$ to 1000 MHz, by analogy with the results on $(H_2O)_2$.

G. DHO—HOH

The energy level diagram for DHO—HOH is shown in Fig. 9. The molecular symmetry group for DHO—HOH is isomorphic to the molecular symmetry groups of HOH—DOH, HOH—HOD, DOD—HOD, and DOD—DOH. However, here we follow Coudert and Hougen (36) and use the species labels A^+, B^+, A^-, and B^- for DHO—HOH instead of the A_1^+, A_1^-, A_2^+, and A_2^- labels used for HOH—DOH, HOH—HOD, DOD—HOD, and DOD—DOH, to reflect the fact that DHO—HOH does not have a plane of symmetry in its equilibrium configuration. The absence of this plane of symmetry allows the observation of additional transitions, driven by the nonzero dipole moment normal to the O—HOH equilibrium plane. Although such transitions were not assigned in the present study, they have been ob-

TABLE 6
Measured Transition Frequencies for D_2O—HOD^a

n^b	$J_{K_aK_c}$	s	n	$J_{K_aK_c}$	s	ν (MHz)	n	$J_{K_aK_c}$	s	n	$J_{K_aK_c}$	s	ν (MHz)
3	1_{10}	A_1^-	3	1_{11}	A_1^+	31.96	3	3_{13}	A_1^+	0	3_{03}	A_1^-	160134.15
3	2_{11}	A_1^+	3	2_{12}	A_1^-	96.03	3	2_{12}	A_1^-	0	2_{02}	A_1^+	160180.48
3	3_{12}	A_1^-	3	3_{13}	A_1^+	192.07	3	1_{11}	A_1^+	0	1_{01}	A_1^-	160211.42
3	4_{13}	A_1^+	3	4_{14}	A_1^-	320.19	3	1_{10}	A_1^-	0	0_{00}	A_1^+	171113.12
3	2_{11}	A_1^+	3	1_{10}	A_1^-	21772.26	3	2_{11}	A_1^+	0	1_{01}	A_1^-	182015.52
0	3_{03}	A_1^-	0	2_{02}	A_1^+	32606.39	3	3_{12}	A_1^-	0	2_{02}	A_1^+	192932.33
3	3_{12}	A_1^-	3	2_{11}	A_1^+	32656.21	3	4_{13}	A_1^+	0	3_{03}	A_1^-	203863.90
0	4_{04}	A_1^+	0	3_{03}	A_1^-	43471.03	3	5_{14}	A_1^-	0	4_{04}	A_1^+	214807.88
3	4_{13}	A_1^+	0	5_{05}	A_1^-	106060.50	3	6_{15}	A_1^+	0	5_{05}	A_1^-	225764.31

^{a} Uncertainties are 0.25 MHz. For transitions given with three digits to the right of the decimal point the uncertainties are 0.01 MHz.
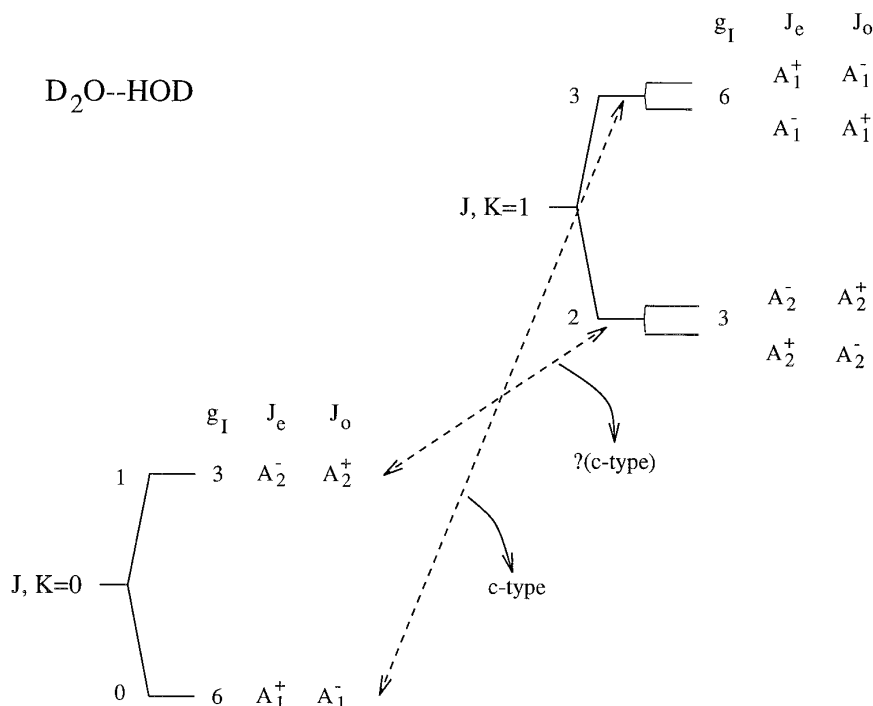^{b} Refer to Figure 6 for definition of n.

D$_2$O--HOD

		g_I	J_e	J_o
	3	6	A_1^+	A_1^-
			A_1^-	A_1^+

J, K=1

			A_2^-	A_2^+
	2	3	A_2^+	A_2^-

?(c-type)

g_I	J_e	J_o
1	3	A_2^-	A_2^+

J, K=0

c-type

| 0 | 6 | A_1^+ | A_1^- |

FIG. 7. Energy-level diagram for D$_2$O—HOD. The band marked with a ''?'' was not assigned in the present investigation.

served previously for DHO—DOD, DHO—HOD, and DHO—DOH, and allow a direct measure of the $K_a = 0$ tunneling splitting associated with the methyl-amine motion. In our previous study of DHO—DOH a strong Coriolis interaction between the $K_a = 0$ and 1 states was also observed. This interaction allows the observation of nominally forbidden $K_a = 0-0$ transitions between the symmetric and antisymmetric methyl-amine-type tunneling states. Because DHO—DOH and DHO—HOH only differ by the hydrogen isotope involved in the hydrogen bond, we also expect DHO—HOH to have a strong $K_a = 0-1$ Coriolis interaction. This interaction may be the origin of our difficulty of presenting a complete assignment of the $K_a = 0$ and 1 states of DHO—HOH. Further complicating the spectroscopy is the fact that in contrast to the other isotopomers discussed, the lowest energy states for both nuclear-spin modifications correlate to symmetric methyl-amine tunneling states. Thus, the much higher ($\sim$7 cm^{-1}) antisymmetric methyl-amine tunneling states can collisional relax in the expansion down to symmetric tunneling states, reducing population and thus our sensitivity to states with $n > 1$.

$K_a = 1-0$ transitions were only assigned between states 0 and 7 and between states 1 and 6. The expected c-type transitions from state 5 to 2 and state 4 to 3 were not positively identified; neither were the b-type transitions from state 0 to 4, 1 to 5, 2 to 6 and 3 to 7, which are allowed by the moment normal to the O—HOH plane. The observed

transitions listed in Table 8 were fit, as before, to the energy level expression of equation 1 to yield the spectroscopic constants listed in Table 2. Again, because of spin statistics, the absolute energy difference between states 0 and 1 could not be determined in the present analysis so that E_0 and E_1 were each constrained to zero in the fit. If we proceed as before and assume the proton donor interchange tunneling has a small K_a dependence we estimate this tunneling splitting to be 1809.38 MHz.

H. DHO—DOD

The energy level diagram for DHO—DOD given in Fig. 10 is qualitatively similar to that of DHO—HOH, except for the nuclear-spin statistical weights. We have previously reported on the observation of the $K_a = 1-0$ spectrum of DHO–DOD. These measurements were restricted to transitions originating from states 2 and 3 in Fig. 10. In the present investigation we complete the characterization of the $K_a = 1-0$ spectrum of this isotopomer by observing both b- and c-type $K_a = 1-0$ transitions coming from states 0 and 1. The measured transitions are listed in Table 9 and the constants resulting from the least-squares fit of these transitions to the energy-level expression of Eq. [1] are given in Table 2. The new data gives a direct measure of the methyl-amine-like tunneling splitting for $K_a = 0$ as 107 723.71(11) MHz. This value can be compared to the values of 117 440.97(17) MHz

TABLE 7
Measured Transition Frequencies for H_2O—DOH[a]

n[b]	$J_{K_aK_c}$	s	n	$J_{K_aK_c}$	s	ν (MHz)	n	$J_{K_aK_c}$	s	n	$J_{K_aK_c}$	s	ν (MHz)
3	2_{11}	A_1^-	3	2_{12}	A_1^+	10.40	1	5_{05}	A_2^+	1	4_{04}	A_2^-	61211.74
3	3_{12}	A_1^+	3	3_{13}	A_1^-	20.78	2	5_{15}	A_2^-	2	4_{14}	A_2^+	61342.13
2	1_{10}	A_2^+	2	1_{11}	A_2^-	143.60	0	5_{05}	A_1^-	0	4_{04}	A_1^+	61539.74
2	2_{11}	A_2^-	2	2_{12}	A_2^+	428.53	3	5_{15}	A_1^-	3	4_{14}	A_1^+	61581.16
2	3_{12}	A_2^+	2	3_{13}	A_2^-	851.08	3	5_{14}	A_1^+	3	4_{13}	A_1^-	61597.90
2	4_{13}	A_2^-	2	4_{14}	A_2^+	1404.90	2	5_{14}	A_2^+	2	4_{13}	A_2^-	62020.85
2	5_{14}	A_2^+	2	5_{15}	A_2^-	2083.55	2	4_{13}	A_2^-	1	3_{03}	A_2^+	72935.38
1	1_{01}	A_2^+	1	0_{00}	A_2^-	12239.001	2	5_{14}	A_2^+	1	4_{04}	A_2^-	85991.08
0	1_{01}	A_1^-	0	0_{00}	A_1^+	12312.523	2	6_{15}	A_2^-	1	5_{05}	A_2^+	99174.27
2	1_{11}	A_2^-	1	1_{01}	A_2^+	22291.63	3	3_{13}	A_1^-	0	4_{04}	A_1^+	369752.19
2	2_{12}	A_2^+	1	2_{02}	A_2^-	22357.17	3	2_{12}	A_1^+	0	3_{03}	A_1^-	382033.52
2	3_{13}	A_2^-	1	3_{03}	A_2^+	22450.30	3	1_{11}	A_1^-	0	2_{02}	A_1^+	394326.48
2	4_{14}	A_2^+	1	4_{04}	A_2^-	22565.43	3	1_{10}	A_1^+	0	1_{01}	A_1^-	418953.90
1	2_{02}	A_2^-	1	1_{01}	A_2^+	24479.057	3	2_{11}	A_1^-	0	2_{02}	A_1^+	418976.90
0	2_{02}	A_1^+	0	1_{01}	A_1^-	24623.903	3	3_{12}	A_1^+	0	3_{03}	A_1^-	419011.40
3	2_{12}	A_1^+	3	1_{11}	A_1^-	24640.08	3	4_{13}	A_1^-	0	4_{04}	A_1^+	419057.80
2	2_{11}	A_2^-	2	1_{10}	A_2^+	24829.60	3	5_{14}	A_1^+	0	5_{05}	A_1^-	419115.50
1	3_{03}	A_2^+	1	2_{02}	A_2^-	36720.94	3	6_{15}	A_1^-	0	6_{06}	A_1^+	419185.60
0	3_{03}	A_1^-	0	2_{02}	A_1^+	36932.94	3	7_{16}	A_1^+	0	7_{07}	A_1^-	419267.00
3	3_{13}	A_1^-	3	2_{12}	A_1^+	36958.07	3	1_{11}	A_1^-	0	0_{00}	A_1^+	431262.30
2	3_{12}	A_2^+	2	2_{11}	A_2^-	37236.45	3	2_{12}	A_1^+	0	1_{01}	A_1^-	443591.40
2	3_{12}	A_2^+	1	2_{02}	A_2^-	60022.33	3	3_{13}	A_1^-	0	2_{02}	A_1^+	455924.50

[a] Uncertainties are 0.25 MHz. For transitions given with three digits to the right of the decimal point the uncertainties are 0.01 MHz.
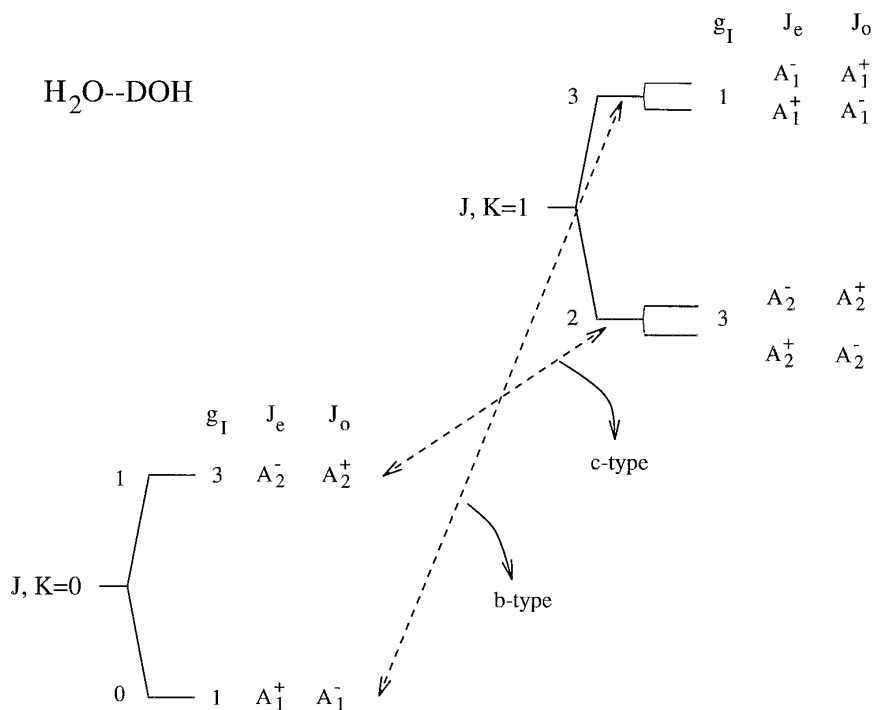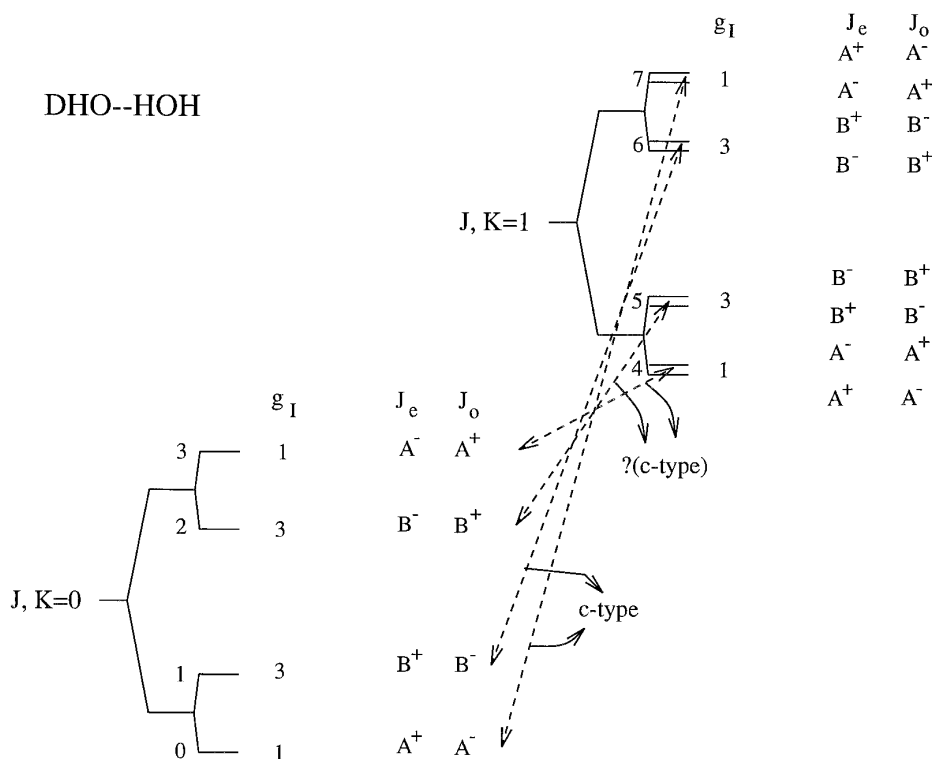[b] Refer to Figure 8 for definition of n.

TABLE 8
Measured Transition Frequencies for DHO—HOH[a]

n[b]	$J_{K_aK_c}$	s	n	$J_{K_aK_c}$	s	ν (MHz)	n	$J_{K_aK_c}$	s	n	$J_{K_aK_c}$	s	ν (MHz)
7	1_{10}	A^-	7	1_{11}	A^+	47.63	6	1_{10}	B^-	1	2_{02}	B^+	329395.95
6	1_{10}	B^-	6	1_{11}	B^+	48.90	7	1_{10}	A^-	0	2_{02}	A^+	333013.72
7	2_{11}	A^+	7	2_{12}	A^-	142.98	6	6_{16}	B^-	1	6_{06}	B^+	352508.90
6	2_{11}	B^+	6	2_{12}	B^-	146.63	6	5_{15}	B^+	1	5_{05}	B^-	352645.20
7	3_{12}	A^-	7	3_{13}	A^+	286.04	6	4_{14}	B^-	1	4_{04}	B^+	352759.42
6	3_{12}	B^-	6	3_{13}	B^+	293.05	6	3_{13}	B^+	1	3_{03}	B^-	352851.25
6	4_{13}	B^+	6	4_{14}	B^-	488.55	6	2_{12}	B^-	1	2_{02}	B^+	352920.33
1	1_{01}	B^-	1	0_{00}	B^+	11810.297	6	1_{11}	B^+	1	1_{01}	B^-	352966.58
0	1_{01}	A^-	0	0_{00}	A^+	11810.297	7	4_{14}	A^-	0	4_{04}	A^+	356379.48
6	3_{13}	B^+	6	2_{12}	B^-	35357.60	7	3_{13}	A^+	0	3_{03}	A^-	356470.61
7	3_{13}	A^+	7	2_{12}	A^-	35357.60	7	1_{11}	A^+	0	1_{01}	A^-	356585.47
0	3_{03}	A^-	0	2_{02}	A^+	35426.10	6	1_{10}	B^-	1	0_{00}	B^+	364825.80
1	3_{03}	B^-	1	2_{02}	B^+	35426.10	7	1_{10}	A^-	0	0_{00}	A^+	368443.16
0	5_{05}	A^-	0	4_{04}	A^+	59028.13	6	2_{11}	B^+	1	1_{01}	B^-	376686.59
1	5_{05}	B^-	1	4_{04}	B^+	59028.13	7	2_{11}	A^+	0	1_{01}	A^-	380302.07
6	5_{14}	B^-	6	4_{13}	B^+	59157.97	6	3_{12}	B^-	1	2_{02}	B^+	388570.78
6	5_{14}	B^-	1	6_{06}	B^+	282557.20	7	3_{12}	A^-	0	2_{02}	A^+	392183.32
7	5_{14}	A^-	0	6_{06}	A^+	286159.16	6	4_{13}	B^+	1	3_{03}	B^-	400477.66
7	4_{13}	A^+	0	5_{05}	A^-	297827.92	7	4_{13}	A^+	0	3_{03}	A^-	404085.73
6	3_{12}	B^-	1	4_{04}	B^+	305915.26	6	5_{14}	B^-	1	4_{04}	B^+	412405.90
7	2_{11}	A^+	0	3_{03}	A^-	321256.19							

[a] Uncertainties are 0.25 MHz. For transitions given with three digits to the right of the decimal point the uncertainties are 0.01 MHz.
[b] Refer to Figure 9 for definition of n.

H$_2$O--DOH

g_I J_e J_o

3 A_1^- A_1^+
1 A_1^+ A_1^-

J, K=1

2 A_2^- A_2^+
3 A_2^+ A_2^-

c-type

g_I J_e J_o

1 3 A_2^- A_2^+

J, K=0

b-type

0 1 A_1^+ A_1^-

FIG. 8. Energy-level diagram for H$_2$O—DOH.

DHO--HOH

g_I J_e J_o
A^+ A^-

7 1 A^- A^+
B^+ B^-
6 3 B^- B^+

J, K=1

5 3 B^- B^+
B^+ B^-
A^- A^+
4 1 A^+ A^-

?(c-type)

g_I J_e J_o
3 1 A^- A^+

2 3 B^- B^+

J, K=0

c-type

1 3 B^+ B^-

0 1 A^+ A^-

FIG. 9. Energy-level diagram for DHO—HOH. Unlike the other isotopomers studied, DHO—HOH does not have a plane of symmetry.
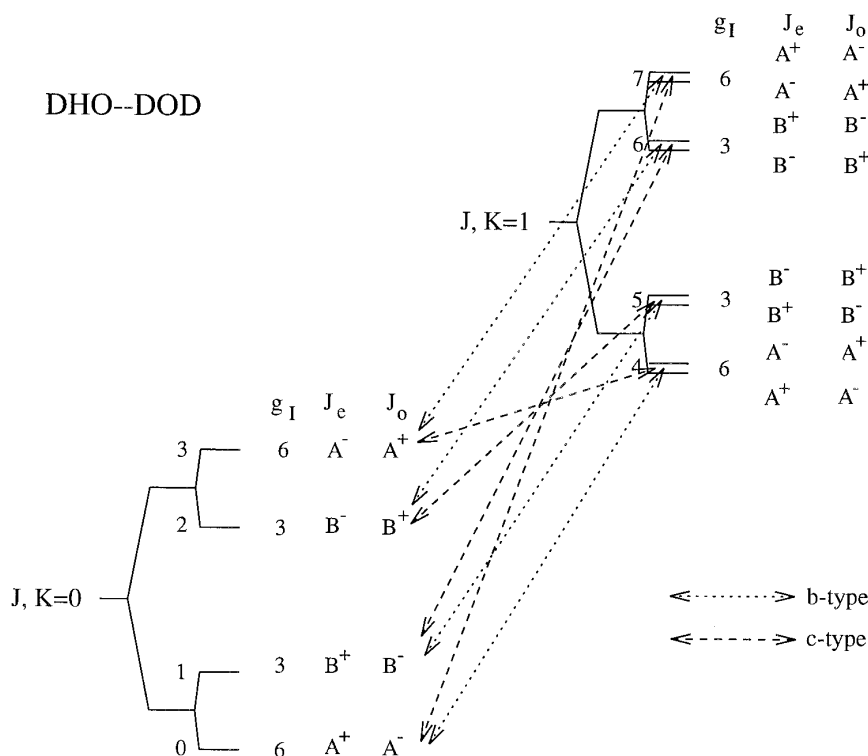
FIG. 10. Energy-level diagram for DHO—DOD.

(*31*) and 214 208.38(23) MHz (*31*) that were previously determined for DHO—HOD and DHO—DOH, respectively. Again, we see that the values for this tunneling splitting are similar for isotopomers which only differ by isotopic substitution of the proton donor hydrogen or deuteron.

IV. DISCUSSION

From the present study we now have precision spectroscopic data on all 12 possible deuterated–protonated isotopomers of water dimer. For isotopomers formed from the same isotopic monomer progenitors, the different possible isomers, such as H_2O—DOD and D_2O—HOH, appear to correspond to *distinct* minima on the same effective potential energy surface, with no evidence observed for any dynamical coupling between these isomers. This contrasts with the case of the isotopic acetylene dimers where a strong anharmonic resonance is observed between the DCCH—DCCD and DCCD—DCCH isotopomers (*52*).

The availability of spectroscopic data on all 12 of the mixed deuterated–protonated isotopomers of water dimer gives new information on the structure of the dimer. In principal, this data, together with results on the ^{17}O- and ^{18}O-containing species, allows the determination of a complete substitution structure for the dimer. Complicating the use of such a procedure is the presence of large-amplitude motions

which effectively average the rotational constants over a large number of angular configurations (as well as radial configurations if radial–angular coupling is significant). In addition, the rotational constants are also ''contaminated'' by Coriolis interactions associated with the large-amplitude motions. Here, we ignore these concerns and least-squares fit the $B + C$ rotational constants known for nine H-bonded species to an O—H hydrogen-bond length ($R_{O—H}$), and O—H–O hydrogen-bond angle ($\angle O—H–O$), and the tilt angle between the proton acceptor two-fold axis and the O—H bond ($\angle C_2–O—H$). $\angle O—H–O$ angles of less than 180° correspond to having the oxygen of the proton donor moving away from the protons of the acceptor while $\angle C_2–$ O—H angles between 90° and 180° correspond to having the hydrogens of the proton acceptor pointing away from the proton donor. In the analysis we also independently fit the 6 D-bonded species to the same parameters. The isotopomers fit include ^{17}O and ^{18}O species. The choice of independently fitting the O—H and O—D bonded species was made due to the dramatic difference in zeropoint binding energy for these species, with the expectation that this difference may be reflected in different effective structural parameters for the two sets of isotopomers.

In the structural analysis, the monomer OH/OD bond lengths and monomer valence angle are fixed at 0.9565 Å and 104.87°, respectively. For the O—H bonded species we

TABLE 9
Measured Transition Frequencies for DHO—DOD[a]

n^b	$J_{K_aK_c}$	s	n	$J_{K_aK_c}$	s	ν (MHz)	n	$J_{K_aK_c}$	s	n	$J_{K_aK_c}$	s	ν (MHz)
6	1_{10}	B^-	6	1_{11}	B^+	17.90	6	6_{15}	B^+	2	6_{06}	B^-	112212.12
7	2_{11}	A^+	7	2_{12}	A^-	53.28	4	4_{13}	A^-	3	3_{03}	A^+	114591.60
4	2_{11}	A^-	4	2_{12}	A^+	183.90	5	4_{13}	B^-	2	3_{03}	B^+	114613.07
3	1_{01}	A^+	3	0_{00}	A^-	11290.200	6	4_{13}	B^+	1	5_{05}	B^-	163311.30
0	1_{01}	A^-	0	0_{00}	A^+	11296.385	7	4_{13}	A^+	0	5_{05}	A^-	163334.07
1	1_{01}	B^-	1	0_{00}	B^+	11296.385	7	5_{15}	A^+	3	4_{04}	A^-	168323.86
5	2_{12}	B^+	5	1_{11}	B^-	22538.10	6	5_{15}	B^+	2	4_{04}	B^-	168332.57
4	2_{12}	A^+	4	1_{11}	A^-	22538.10	6	3_{12}	B^-	1	4_{04}	B^+	174591.28
3	2_{02}	A^-	3	1_{01}	A^+	22579.55	7	3_{12}	A^-	0	4_{04}	A^+	174615.59
2	2_{02}	B^-	2	1_{01}	B^+	22579.55	5	1_{10}	B^+	1	1_{01}	B^-	176798.13
0	2_{02}	A^+	0	1_{01}	A^-	22591.793	4	1_{10}	A^+	0	1_{01}	A^-	176809.67
1	2_{02}	B^+	1	1_{01}	B^-	22591.793	5	2_{11}	B^-	1	2_{02}	B^+	176866.97
6	2_{11}	B^+	6	1_{10}	B^-	22595.10	4	2_{11}	A^-	0	2_{02}	A^+	176878.45
7	2_{11}	A^+	7	1_{10}	A^-	22595.10	5	3_{12}	B^+	1	3_{03}	B^-	176970.08
7	3_{13}	A^+	7	2_{12}	A^-	33837.20	4	3_{12}	A^+	0	3_{03}	A^-	176981.44
6	3_{13}	B^+	6	2_{12}	B^-	33837.20	5	4_{13}	B^-	1	4_{04}	B^+	177107.52
0	3_{03}	A^-	0	2_{02}	A^+	33885.50	4	4_{13}	A^-	0	4_{04}	A^+	177118.75
1	3_{03}	B^-	1	2_{02}	B^+	33885.50	5	5_{14}	B^+	1	5_{05}	B^-	177279.04
6	3_{12}	B^-	6	2_{11}	B^+	33890.40	4	5_{14}	A^+	0	5_{05}	A^-	177290.08
7	3_{12}	A^-	7	2_{11}	A^+	33890.40	5	6_{15}	B^-	1	6_{06}	B^+	177484.42
4	3_{12}	A^+	4	2_{11}	A^-	33988.56	4	6_{15}	A^-	0	6_{06}	A^+	177495.28
5	3_{12}	B^+	5	2_{11}	B^-	33988.56	5	7_{16}	B^+	1	7_{07}	B^-	177723.64
4	2_{11}	A^-	3	3_{03}	A^+	35289.44	4	7_{16}	A^+	0	7_{07}	A^-	177734.08
3	5_{05}	A^+	3	4_{04}	A^-	56432.80	4	8_{17}	A^-	0	8_{08}	A^+	178006.60
1	5_{05}	B^-	1	4_{04}	B^+	56463.16	7	6_{16}	A^-	3	5_{05}	A^+	179540.70
0	5_{05}	A^-	0	4_{04}	A^+	56463.16	6	6_{16}	B^-	2	5_{05}	B^+	179549.16
4	4_{14}	A^+	3	4_{04}	A^-	68827.42	6	2_{11}	B^+	1	3_{03}	B^-	185876.90
5	4_{14}	B^+	2	4_{04}	B^-	68849.20	7	2_{11}	A^+	0	3_{03}	A^-	185900.36
4	3_{13}	A^-	3	3_{03}	A^+	68910.31	5	1_{11}	B^-	1	0_{00}	B^+	188032.99
5	3_{13}	B^-	2	3_{03}	B^+	68932.17	4	1_{11}	A^-	0	0_{00}	A^+	188044.75
4	2_{12}	A^+	3	2_{02}	A^-	68972.45	6	1_{10}	B^-	1	2_{02}	B^+	197166.45
5	2_{12}	B^+	2	2_{02}	B^-	68994.37	5	2_{12}	B^+	1	1_{01}	B^-	199274.39
4	1_{11}	A^-	3	1_{01}	A^+	69013.83	4	2_{12}	A^+	0	1_{01}	A^-	199286.84
5	1_{11}	B^-	2	1_{01}	B^+	69035.81	7	8_{18}	A^-	3	7_{07}	A^+	201926.30
7	2_{12}	A^-	3	3_{03}	A^+	78143.63	4	3_{13}	A^-	0	2_{02}	A^+	210499.21
6	2_{12}	B^-	2	3_{03}	B^+	78152.56	6	4_{14}	B^-	1	4_{04}	B^+	219596.13
4	1_{10}	A^+	3	0_{00}	A^-	80365.53	7	3_{13}	A^+	0	3_{03}	A^-	219684.14
5	1_{10}	B^+	2	0_{00}	B^-	80387.42	6	2_{12}	B^-	1	2_{02}	B^+	219708.33
7	1_{11}	A^+	3	2_{02}	A^-	89451.07	7	2_{12}	A^-	0	2_{02}	A^+	219732.55
6	1_{11}	B^+	2	2_{02}	B^-	89460.12	6	1_{11}	B^+	1	1_{01}	B^-	219740.35
4	2_{11}	A^-	3	1_{01}	A^+	91735.94	7	1_{11}	A^+	0	1_{01}	A^-	219764.95
5	2_{11}	B^-	2	1_{01}	B^+	91757.84	5	4_{14}	B^+	1	3_{03}	B^-	221671.90
4	3_{12}	A^+	3	2_{02}	A^-	103144.98	4	4_{14}	A^+	0	3_{03}	A^-	221683.00
5	3_{12}	B^+	2	2_{02}	B^-	103166.73	6	1_{10}	B^-	1	0_{00}	B^+	231054.79
7	1_{10}	A^-	3	1_{01}	A^+	112048.28	5	5_{15}	B^-	1	4_{04}	B^+	232824.97
6	1_{10}	B^-	2	1_{01}	B^+	112057.52	4	5_{15}	A^-	0	4_{04}	A^+	232835.68
7	2_{11}	A^+	3	2_{02}	A^-	112064.00	6	2_{11}	B^+	1	1_{01}	B^-	242353.70
6	2_{11}	B^+	2	2_{02}	B^-	112073.28	7	2_{11}	A^+	0	1_{01}	A^-	242377.79
7	3_{12}	A^-	3	3_{03}	A^+	112087.44	6	3_{12}	B^-	1	2_{02}	B^+	253652.57
6	3_{12}	B^-	2	3_{03}	B^+	112096.72	7	3_{12}	A^-	0	2_{02}	A^+	253676.58
7	4_{13}	A^+	3	4_{04}	A^-	112118.40	6	4_{13}	B^+	1	3_{03}	B^-	264950.40
6	4_{13}	B^+	2	4_{04}	B^-	112127.88	7	4_{13}	A^+	0	3_{03}	A^-	264973.76
7	5_{14}	A^-	3	5_{05}	A^+	112156.92	7	5_{14}	A^-	0	4_{04}	A^+	276269.00
6	5_{14}	B^-	2	5_{05}	B^+	112166.36	6	6_{15}	B^+	1	5_{05}	B^-	287539.00
7	6_{15}	A^+	3	6_{06}	A^-	112202.64	7	6_{15}	A^+	0	5_{05}	A^-	287561.18

[a] Uncertainties are 0.25 MHz. For transitions given with three digits to the right of the decimal point the uncertainties are 0.01 MHz.
[b] Refer to Figure 10 for definition of n.

find $R_{O-H} = 2.0164(18)$ Å, $\angle O-H-O = 183.8(16)°$, and $\angle C_2-O-H = 126.2(10)°$, while for the O—D bonded species we find $R_{O-H} = 2.0148(11)$ Å, $\angle O-H-O = 183.1(8)°$, and $\angle C_2-O-H = 124.0(10)°$. Both the ''statistical'' uncertainties on the parameters and the difference in lengths and angles between the two data sets give an indication of the magnitude of the errors resulting from neglect of a complete treatment of the large-amplitude motions.

Recently, Gregory and Clary (9) have undertaken diffusion Monte Carlo calculations of tunneling splittings of mixed deuterated-protonated water dimers using the anisotropic site potential of Millot and Stone (53). For HDO—DOD and HDO—DOH we can compare the predicted and calculated values for the methyl-amine type tunneling splitting since the experimental measurements directly probe this splitting for $J = 0$. In the present work we find a tunneling splitting of 3.59 cm^{-1} for HDO—DOD and previously (31) we obtained a value of 7.15 cm^{-1} for HDO—DOH. Gregory and Clary (9) find significantly smaller values for these splittings of 2.6(4) and 2.4(4) cm^{-1}, respectively. Their calculations indicate that the potential is much to stiff in the internal-rotation coordinate. Gregory and Clary (9) report similar calculations for several of the other isotopomers of water dimer, however, for these species a direct measure of the methyl-amine tunneling splitting is not available due to symmetry restrictions on the transition selection rules.

Gregory and Clary (9) also present calculations of the proton-donor interchange tunneling splitting for the $K_a = 0$ symmetric methyl-amine tunneling states of HDO—DOD and H$_2$O—DOD of 0.0012(4) and 0.0014(4) cm^{-1}, respectively. Because of the rotation-tunneling selection rules, our measurements do not directly probe this splitting, however the calculated splittings are in reasonable agreement with the values of 0.0008 cm^{-1} for H$_2$O—DOD averaged over the $K_a = 0$ and 1 states, and the 0.0006 cm^{-1} value for HDO—DOD averaged over the two $K_a = 0$ methyl-amine tunneling states.

V. CONCLUSION

As discussed above, the present measurements provide an extensive data set to test proposed intermolecular potentials for water. Gregory and Clary (9) have calculated $J = 0$ tunneling splittings for a number of isotopomers of water dimer. To calculate energy levels for higher J levels requires significant increases in computational resources. For the C_s-symmetry isotopomers the $J = 0$ methyl-amine-type tunneling splittings are not directly measured experimentally, but must be inferred from a suitable fit to a model Hamiltonian. Coudert and Hougen (38) have developed a model Hamiltonian which allows the determination of the $J = 0$ tunneling splittings, under the assumption that the tunneling dynamics is in the high-barrier limit. To determine the $J = 0$ tunneling

splitting correctly it is necessary that the Hamiltonian correctly models the large K_a dependence to this splitting. The present data set and our previous measurements on water dimer complexes in which an HDO subunit is the acceptor should allow a direct test of the Coudert and Hougen (38) model since for these complexes the selection rules allow for the methyl-amine-like tunneling splitting to be precisely measured. In addition, the large number of measurements on the various isotopomers of the water dimer may motivate future efforts at developing spectroscopic Hamiltonians for multidimensional tunneling problems necessary to allow more complete comparisons between theory and experiment.

REFERENCES

1. For recent reviews, see: J. M. Hutson, *Annu. Rev. Phys. Chem.* **41,** 123–154 (1990) and R. C. Cohen and R. J. Saykally, *Annu. Rev. Phys. Chem.* **42,** 369–392 (1991).

2. A. E. Barton and B. J. Howard, *Faraday Discuss. Chem. Soc.* **73,** 45–62 (1982).

3. M. Quack and M. Suhm, *J. Chem. Phys.* **95,** 28–59 (1991).

4. M. J. Elrod and R. J. Saykally, *J. Chem. Phys.* **103,** 933–949 (1995).

5. F.-M. Tao and W. Klemperer, *J. Chem. Phys.* **99,** 5976–5982 (1993), and references therein.

6. E. H. T. Olthof, A. van der Avoird, and P. E. S. Wormer, *J. Chem. Phys.* **101,** 8430–8442 (1994), and references therein.

7. S. C. Althorpe and D. C. Clary, *J. Chem. Phys.* **101,** 3603–3609 (1994).

8. S. C. Althorpe and D. C. Clary, *J. Chem. Phys.* **102,** 4390–4399 (1994).

9. J. K. Gregory and D. C. Clary, *J. Chem. Phys.* **102,** 7817–7829 (1995).

10. T. R. Dyke and J. S. Muenter, *J. Chem. Phys.* **60,** 2929–2930 (1974).

11. T. R. Dyke, K. M. Mack, and J. S. Muenter, *J. Chem. Phys.* **66,** 498–510 (1977).

12. J. A. Odutola and T. R. Dyke, *J. Chem. Phys.* **72,** 5062–5070 (1980).

13. L. H. Coudert, F. J. Lovas, R. D. Suenram, and J. T. Hougen, *J. Chem. Phys.* **87,** 6290–6299 (1987).

14. T. R. Dyke, *in* ''Structure and Dynamics of Weakly Bound Molecular Complexes'' (A. Weber, Ed.), pp. 43–56. Reidel, Boston, 1987.

15. Z. S. Huang and R. E. Miller, *J. Chem. Phys.* **88,** 8008–8009 (1988).

16. J. A. Odutola, T. A. Hu, D. Prinslow, S. E. O'dell, and T. R. Dyke, *J. Chem. Phys.* **88,** 5352–5361 (1988).

17. L. Martinache, S. Jans-Bürli, B. Vogelsanger, W. Kresa, and A. Bauder, *Chem. Phys. Lett.* **149,** 424–428 (1988).

18. G. T. Fraser, R. D. Suenram, L. H. Coudert, and R. S. Frye, *J. Mol. Spectrosc.* **137,** 244–247 (1989).

19. K. L. Busarow, R. C. Cohen, G. A. Blake, K. B. Laughlin, Y. T. Lee, and R. J. Saykally, *J. Chem. Phys.* **90,** 3937–3943 (1989).

20. G. T. Fraser, R. D. Suenram, L. H. Coudert, *J. Chem. Phys.* **90,** 6077–6085 (1989).

21. Z. S. Huang and R. E. Miller, *J. Chem. Phys.* **91,** 6613–6631 (1989).

22. R. D. Suenram, G. T. Fraser, and F. J. Lovas, *J. Mol. Spectrosc.* **138,** 440–449 (1989).

23. T. A. Hu and T. R. Dyke, *J. Chem. Phys.* **91,** 7348–7354 (1989).

24. E. Zwart, J. J. ter Meulen, and W. L. Meerts, *Chem. Phys. Lett.* **166,** 500–502 (1990).

25. E. Zwart, J. J. ter Meulen, and W. L. Meerts, *Chem. Phys. Lett.* **173,** 115–121 (1990).

26. N. Pugliano and R. J. Saykally, *J. Chem. Phys.* **96,** 1832–1839 (1992).

27. E. N. Karyakin, G. T. Fraser, and R. D. Suenram, *Mol. Phys.* **78,** 1179–1189 (1993).

28. W. Stahl and L. H. Coudert, *J. Mol. Phys.* **157,** 161–171 (1993).

29. N. Pugliano, J. D. Cruzan, J. G. Loeser, and R. J. Saykally, *J. Chem. Phys.* **98,** 6600–6617 (1993).

30. E. N. Karyakin, G. T. Fraser, B. H. Pate, and R. D. Suenram, *J. Mol. Spectrosc.* **161,** 213–9316 (1993).

31. E. N. Karyakin, G. T. Fraser, F. J. Lovas, R. D. Suenram, and M. Fujitake, *J. Chem. Phys.* **102,** 1114–1121 (1995).

32. G. T. Fraser, *Int. Rev. Phys. Chem.* **10,** 189–206 (1991).

33. T. R. Dyke, *J. Chem. Phys.* **66,** 492–497 (1977).

34. J. T. Hougen, *J. Mol. Spectrosc.* **114,** 395–426 (1985).

35. D. D. Nelson, Jr., and W. Klemperer, *J. Chem. Phys.* **87,** 139–149 (1987).

36. L. H. Coudert and J. T. Hougen, *J. Mol. Spectrosc.* **130,** 86–119 (1988).

37. B. J. Smith, D. J. Swanton, J. A. Pople, H. F. Schaefer III, and L. Radom, *J. Chem. Phys.* **92,** 1240–1247 (1990).

38. L. H. Coudert and J. T. Hougen, *J. Mol. Spectrosc.* **139,** 259–277 (1990).

39. R. E. Bumgarner, S. Suzuki, P. A. Stockman, P. G. Green, and G. A. Blake, *Chem. Phys. Lett.* **176,** 123–127 (1991).

40. P. A. Stockman, R. E. Bumgarner, S. Suzuki, and G. A. Blake, *J. Chem. Phys.* **96,** 2496–2510 (1992).

41. G. T. Fraser and A. S. Pine, **91,** 637–645 (1989).

42. T. E. Gough, R. E. Miller, and G. Scoles, *Appl. Phys. Lett.* **30,** 338–340 (1977).

43. G. T. Fraser, A. S. Pine, J. L. Domenech, and B. H. Pate, *J. Chem. Phys.* **99,** 2396–2404 (1993).

44. Yu. I. Alekshin, G. M. Altshuller, O. P. Pavlovsky, E. N. Karyakin, A. F. Krupnov, D. G. Paveliev, and A. P. Shkaev, *Int. J. Infrared Millimeter Waves,* **11,** 961–971 (1990).

45. T. J. Balle and W. H. Flygare, *Rev. Sci. Instrum.* **52,** 33–45 (1981).

46. K. M. Evenson, D. A. Jennings, and F. R. Peterson, *Appl. Phys. Lett.* **44,** 576–578 (1984).

47. F. J. Lovas and R. D. Suenram, *J. Chem. Phys.* **87,** 2010–2020 (1987).

48. R. D. Suenram, F. J. Lovas, G. T. Fraser, J. Z. Gillies, C. W. Gillies, and M. Onda, *J. Mol. Spectrosc.* **137,** 127–137 (1989).

49. F. J. Lovas, N. Zobov, G. T. Fraser, and R. D. Suenram, *J. Mol. Spectrosc.* **171,** 189–199 (1995).

50. D. W. Firth, M. A. Dvorak, S. W. Reeve, R. S. Ford, K. R. Leopold, *Chem. Phys. Lett.* **168,** 161–167 (1990).

51. D. W. Firth, K. Beyer, M. A. Dvorak, S. W. Reeve, A. Grushow, and K. R. Leopold, *J. Chem. Phys.* **94,** 1812–1819 (1991).

52. K. Matsumura, F. J. Lovas, and R. D. Suenram, *J. Mol. Spectrosc.* **150,** 576–596 (1991).

53. C. Millot and A. J. Stone, *Mol. Phys.* **77,** 439–462 (1992).